Theoretical modeling and experimental investigations for the improvement of the mechanical efficiency in sliding vane rotary compressors

Giuseppe Bianchi, Roberto Cipollone*

University of L'Aquila, Department of Industrial and Information Engineering and Economics, Via Giovanni Gronchi 18, 67100 L'Aquila, Italy

Abstract

Positive displacement compressors lead the market of compressed air production for industrial applications. Among them, sliding vane rotary compressors represent an energetically virtuous alternative to the current compression technologies. In the present work, the effects of compressor design parameters were investigated through a comprehensive approach that aimed at addressing more efficient machines to promote sliding vane compressors as the key enabling technology in compressed air systems. A comprehensive mathematical model was developed to study the main phenomena occurring in this kind of compressors. The model provides the cell volume evolution over a whole rotation during which filling, compression and discharge processes occur. The first and latter phases are described by the quasi-propagatory approach that represents the inertial, capacitive and resistive features of one-dimensional unsteady flows. The dynamics of the compressor blades led to four different arrangements inside the rotor slots while an analysis of the hydrodynamic lubrication established between blade tip and stator wall focused on the oil film thickness evolution to prevent dry contacts. An extensive experimental campaign on a mid-size industrial compressor allowed the model validation at different outlet pressure levels and revolution speeds using a direct measurement of mechanical power and the reconstruction of the indicator diagram from piezoelectric pressure transducers. The friction coefficient at the contact points between blades with stator and rotor was estimated in 0.065 and further improvements of the mechanical efficiency were eventually addressed considering the roles of compressor aspect ratio, revolution speed, and blade tilt. The first two theoretical optimizations might lead to an increase of the compressor efficiency of 2 and 9 percentage points respectively. On the other hand, acting on the blade tilt would not produce relevant improvements.

Keywords: sliding vane rotary compressor, positive displacement compressor, compressed air systems, indicator diagram, piezoelectric pressure transducer, mechanical efficiency

*Corresponding author

Email addresses: giuseppe.bianchi@graduate.univaq.it (Giuseppe Bianchi), roberto.cipollone@univaq.it (Roberto Cipollone)

1. Introduction

Energy saving is today recognized as the primary action to accomplish energetic and environmental commitments of all the Countries in the World. CO_2 concentration in atmosphere is a crucial concern, universally recognized as the tomorrow's main challenge. Therefore, a new energy paradigm based on a sharp reduction of the energy consumptions and a renewable-based energy production is sought by many scientific and institutional contexts.

Compressed air accounts for a mean 10 % of the global industrial electricity consumptions (7850 TWh in 2012) which reaches a share close to 20 % if commercial and residential needs are included [1, 2, 3]. Facing this issue implies the employment of many saving measures with actions upstream and downstream of the compressed air production: pipeline leakages reduction, adjustable speed drives, optimization of the end use devices, etc. In addition, with reference to electricity consumptions in compressed air systems, the saving potential related to compressor technology has been estimated 25-30 % [1]. From an economic point of view, although energy costs for compressed air are predominant with respect to the capital ones (70-75 %) [2], an investment increase of 10 % in a 10 year operating period would be feasible only if the compressor efficiency increase was 4 % greater than the former technology [3].

In industrial applications, rotary volumetric compressors are able to match flow rate and pressure level requirements with an electrical power range from a few to several hundred kilowatts. Among them, Sliding Vane Rotary Compressors (SVRC) revealed a better energetic behavior whether on/off load conditions were taken into account [3]. This operating regime is a common process to match the line pressure needs in terms of flow rate: when the air demand decreases, thanks to the automatic depressurization of the machine and some intrinsic features related to the sealing among vanes (e.g. absence of the so called "blow hole line"), SVRCs accomplish in an efficient way a process that is usually energy wasteful.

In the literature, sliding vane compressors have been investigated both theoretically and experimentally. The machine geometry and vane kinematics were modeled following a trigonometric approach [4, 5]. Circular and elliptical stator configurations to achieve higher volumetric ratios or even dual stage compressions were considered [6, 7] as well as slanted blade arrangements inside the rotor slots [8, 9]. Preliminary studies assumed suction and discharge processes as isobaric while the compression was modeled using semi-empirical formulations [6]. However, zero dimensional models for the cell thermodynamics were also developed based on the energy conservation to predict the pressure evolution over the whole cell rotation [5, 9, 10, 11]. To detail the friction power, the contribution due to the blade dynamics was widely investigated [12, 13]. Comprehensive analyses that involve secondary contributions such as friction at the bearings and on the side covers of the machine [14, 15] or the blade tip profile [16, 17] were also developed. Leakage paths models were presented assuming clearances as orifices [18]. As concerns the experimental activities, tests at different steady conditions [19, 20, 21] and on unconventional configurations like the blade tilting [22] were carried out. Experimental methodologies have been set up to measure the pressure inside the compressor cells [23, 24, 25] while theoretical approaches as the Helmotz's resonator one supported the discussion of the results [26, 27].

Although it deeply focused on specific aspects of the sliding vane compressor technology, the above mentioned literature does not strictly aim at maximizing the overall machine efficiency. This goal is of major concern for sliding vane rotary compressors since the benefits that would come out from an energy performance enhancement might make them as the key enabling technology in compressed air systems. At the moment, there are air flow ranges in which SVRCs are characterized by specific energy consumptions lower than other compressors [3]. The reinforcement of this issue and the broadening of their behavior at wider flow ranges appear the way to refer to these machines as premium ones concerning the energy consumptions. Furthermore, compared to other compression technologies, SVRCs have a relevant improvement potential whose development is referred to friction power reduction and to the internal air cooling during the compression phase [28, 29]. Despite similar methodologies are not currently available in literature, in order to identify the energy saving potential, a wide-ranging approach becomes necessary to understand how the different design parameters can contribute to the machine efficiency. A comprehensive model appears to be the best way to observe cross coupled effects among different design parameters. Once experimentally validated, it behaves as a SVRC virtual platform allowing the addressment of efficiency improvements and, at the same time, the reduction of prototype construction.

The model presented in the current work is composed of a geometrical section that is able to provide the cell volume evolution for any compressor layout in terms of aspect ratio, blade tilt, intake and exhaust ports arrangements. A quasi-propagatory approach described the flow dynamics during the vanes filling and emptying while a lumped parameter model was adopted to predict the pressure evolution over a whole rotation of the compressor cells. The study of the blade dynamics coupled with an analysis of the hydrodynamic lubrication at the blade tip provided the oil film thickness evolution at the interface with the stator wall. The role of reaction forces and pressure distribution along this oil layer is of major importance to account for losses by friction, thus to a proper investigation of the mechanical efficiency of the machine.

An experimental campaign on a mid-size industrial sliding vane compressor was performed at different outlet pressure levels and revolution speed regimes. The direct measurement of mechanical power, as well as the reconstruction of the indicator diagram from pressure data provided by piezoelectric transducers, allowed to validate the model and led to an estimation of the friction coefficient. The pressure distribution along the oil layer at the blade tip was further calculated. Parametric analyses on the effects of aspect ratio, revolution speed, blade tilt and mass on the mechanical efficiency of the compressor, were eventually carried out in order to identify improved configurations that would reduce the energy consumptions.

2. Mathematical model

The main phenomena occurring inside a sliding vane rotary compressor were modeled through an essential formulation: the sliding vane compressor from the suction port till the compressed air line inlet was represented as a sequence of ducts and capacities that exchange mass and energy according to a 1D quasi-propagatory formulation. The compressor core, i.e. the stator rotor and blades assembly, was modeled with a lumped parameter approach. Hence, the compressor cell acted as a volume of variable capacity that interacted with the adjacent cells and with the rest of the compressor through the suction and discharge ports. The solution of the momentum equation for the compressor blades provided an estimation of the friction power that directly affects the machine efficiency. The lubrication circuit modeling and the calculation of the load distribution at the blade tip eventually allowed to estimate the pressure distribution and the oil film thickness evolution along contact surface with the stator. Since the oil sealing in sliding vane compressors is effective, leakage flows modeling (for instance using semi-empirical correlations) was not pursued; this assumption allowed to keep the model platform independent from the compressor tested, thus able to simulate the performances of different machines.

2.1. Compressor geometry

The compressor vane geometry was modeled tracking the trajectories of all the relevant points in the compressor core represented in Figure 1.a. To investigate the effects of the blade tilt onto the mechanical efficiency of the machine, backward and forward slanting were also implemented (Figure 1.b). In these configurations, blades are tangent to an internal circumference whose radius ($O_{rot}A$) is smaller than the rotor one (OX). As concerns the intake and exhaust ports, they are located either frontally (on the covers, with an axial air path) or circumferentially (with a radial air admission or delivery). Regardless of the configuration, the angular ports positioning has a direct influence on the volumetric compression ratio i.e. the ratio between the cell volume before it opens toward the exhaust and the one after closing the inlet port. Although the model can consider ports anyway located, in current industrial compressors the intake is usually axial while the discharge is radial, as reported in Figure 1.c.

2.2. Vane filling and emptying

In order to evaluate the flow dynamics during the intake and exhaust processes, a Quasi Propagatory Model (QPM) was adopted. Based on the 1D unsteady conservation equations, the method solves them in an analytical way taking into account the capacitive (pressure as a function of inlet and outlet mass flow rates), inertial (mass flow variation as a function of a pressure difference) and resistive features (losses by friction and heat exchange) of the flow topology [30]. QPM subdivides complex one dimensional sequence of pipes anyway interconnected into elementary parts, whose extremities are stimulated by boundary conditions (BC) modeled as functions of pressure and flow velocity. The intersection of the curves representing the

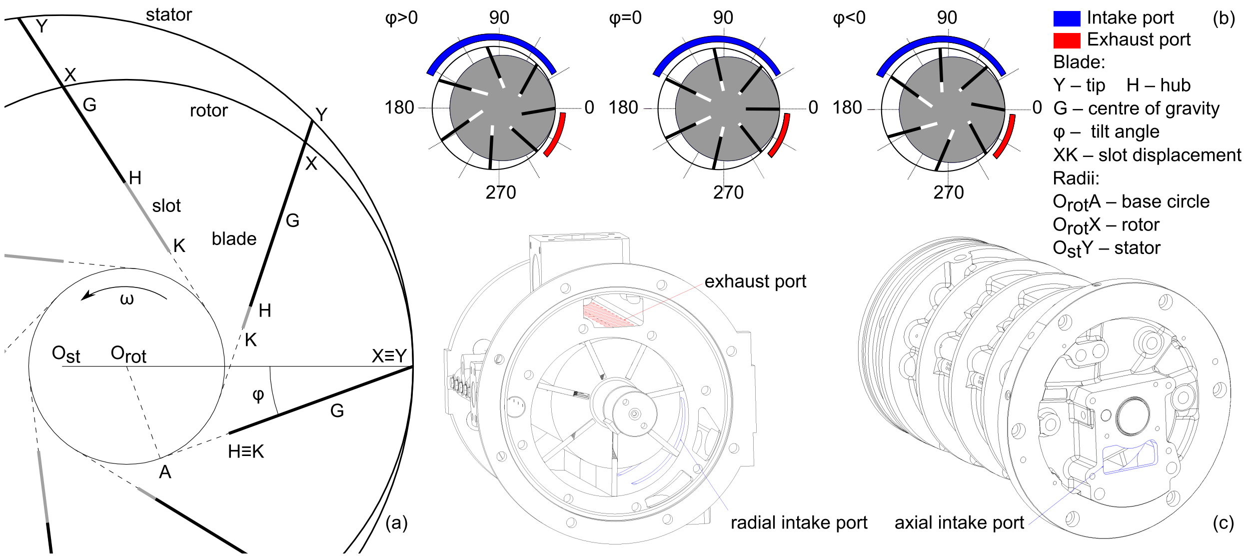

Figure 1: Compressor core - the geometrical modeling is based on the trajectories of the relevant points of the assembly (a) and may take into account forward and backward blade tilting (b) as well as axial and radial ports (c)

upstream and downstream BCs in the $p-u$ plane gives the steady state (SS) of the flow after the transient (Figure 2.a).

To model the dynamics of homentropic flows only the mass and momentum conservation equations are required. The homentropic steady state may be eventually corrected if heat exchange and friction occur [31]. Considering the mid-point of the elementary pipe, the (p,u) solution over time is represented by the sequence of values which result from the pressure (and speed) waves propagation calculated as intersections between the characteristic curves entering the BCs and the BCs themselves. The novelty of the QPM lies on the approximation of the boundary conditions with lines at constant slope (evaluated at the initial state): this allows to linearize and speed up the calculation such that the flow evolution at a given location can be characterized with the Equations 1:

$$p = p_u - \frac{p_u - p_\infty}{u_\infty} u = p_u - A\,u \tag{1a}$$

$$p = p_d - \frac{p_\infty - p_d}{u_\infty} u = p_d + B\,u \tag{1b}$$

The flow dynamics inside the pipe starts from the initial state 0 and proceeds along the characteristic curves bounded by the BCs: 0-1 represents the propagation of the positive characteristic curve while 1-2 is related to the propagation of the negative characteristic curve until the SS, represented by the point (u_∞,p_∞) in Figure 2.a, is reached. The time base is given by the time the waves require to move between successive intermediate states and it is equal to the ratio of the pipe length over the local speed of sound a.

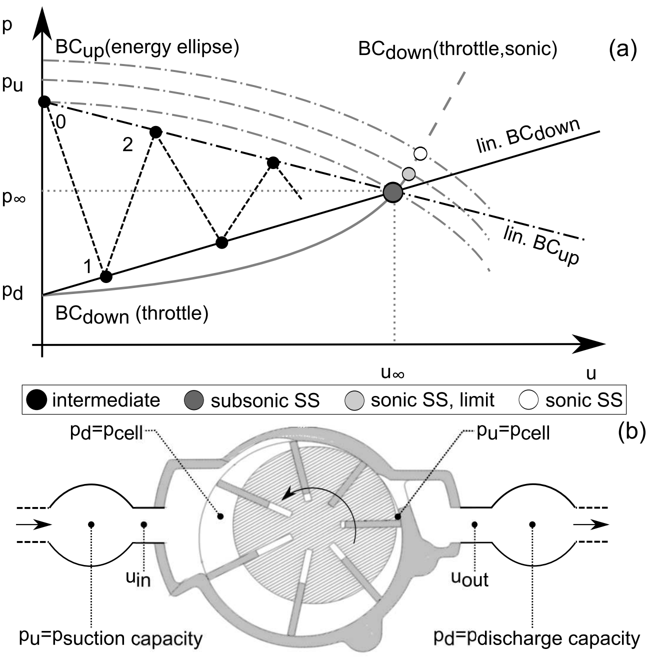

Figure 2: Quasi-propagatory flow dynamics along the suction and discharge compressor ducts

With reference to the initial value of pressure, the slope of the characteristic curves $C = \gamma\, p'/a$ and the linearization of boundary conditions lead to the definition of the parameter Λ:

$$\Lambda = \frac{(C-B)\,(C-A)}{(C+B)\,(C+A)} \tag{2}$$

Depending on the sign of Λ which is strictly related to the set of boundary conditions, the flow dynamics follows either an asymptotical ($\Lambda > 0$ - Eqn. 3) or an oscillatory ($\Lambda < 0$ - Eqn. 4) trend until the steady state is reached:

$$\dot{u} + \frac{u}{\tau} = \frac{u_\infty}{\tau} \tag{3}$$

$$\ddot{u} + \frac{2}{\tau}\dot{u} + \left(\frac{1}{\tau^2} + \Omega^2\right) u = \left(\frac{1}{\tau^2} + \Omega^2\right) u_\infty \tag{4}$$

The parameters Ω and τ depend on the boundary conditions and their slopes when linearized [30].
Once the midpoint velocity is evaluated at a given time step, the mass flow rate in the duct with cross section S can be calculated according to Eqn. 5:

$$\dot{m} = \rho_\infty\, u\, S = \frac{\gamma\, p_\infty}{{a_\infty}^2}\, u\, S \tag{5}$$

In the compressor model, QPM decomposes the inlet and outlet sections of the compressor as a series of ducts and reservoirs. To model the unsteadiness of vane filling and emptying, infinitesimal ducts were considered between the cells and the suction and discharge capacities, as represented in Figure 2.b. The inlet (u_{in}) and outlet (u_{out}) flow velocities vary with time as the result of the interaction between the upstream and downstream BCs that characterize the intake and exhaust respectively. Both processes were modeled as a reservoir that feeds a throttled duct: with respect to the intake pipe, during the vane filling the environment behaves as a reservoir at ambient pressure while the motion of the compressor cell downstream becomes a flow restriction with variable crossing area. In analytical terms, the energy conservation expressed in terms of total pressure, leads to the energy ellipse for the upstream BC while the throttling action of the cell considers a subsonic (parabolic) stage followed by a sonic one whose trend is linear. Similarly, the emptying process occurs through a pipe that upstream has the discharging cell which acts as a variable flow restriction while downstream it is connected through a plenum at the line pressure. For a given contraction ratio ζ, that depends on the opening of the intake and exhaust ports preliminary evaluated in the geometric module, the steady state is analytically computable according to Eqn. 6.

$$u_\infty^2 = \frac{2\gamma\, RT_u}{\gamma - 1}\zeta^2 \left[1 - \left(\frac{p_d}{p_u}\right)^{\frac{\gamma-1}{\gamma}}\right] \tag{6a}$$

$$p_\infty = p_u \left[1 - \zeta^2 \left[1 - \left(\frac{p_d}{p_u}\right)^{\frac{\gamma-1}{\gamma}}\right]\right]^{\frac{\gamma}{\gamma-1}} \tag{6b}$$

Although the model scheme is the same, the boundary conditions across the suction and discharge ducts are greatly different. Indeed, if the compressor operated at off-design conditions, at the discharge the line pressure might be several bars different than the one in the discharging vane; a sudden pressure step (theoretically isochoric) would thus occur because of the fixed compression ratio which is imposed by the machine geometry. Consequently, the mismatching between pressure at the cell opening and the value of the compressed air line would trigger pressure unsteadiness, with a magnitude proportional to the pressure step. On the other hand, during the vane filling the pressure in the suction capacity is slightly greater than the one in the cell. Therefore, sonic flows might occur whether the cell pressure when it opens towards the suction port is less than 0.5 times the ambient one.

Using an adiabatic-isentropic approach, once the inlet and outlet velocities are known, the density calculation is straightforward as well as all the thermodynamic flow properties (temperature, enthalpy, etc.).

2.3. Cell Thermodynamics

The model is based on a lumped parameter formulation that assumes uniform thermodynamic properties (temperature, pressure, composition, etc.) inside the cell. Considering the lubricant injection, the working fluid is a mixture of air and oil vapors. The cell behaves like an open system, characterized by input and output enthalpy flows that depend on the filling and emptying processes. The first law of the thermodynamics applied to an open system doing only boundary work assumes the expression in Eqn. 7:

$$\dot{E} = \dot{m}_{inl}\, H_{inl} - \dot{m}_{outl}\, H_{outl} - \dot{q}_{air-oil} - \dot{q}_{evap} - \dot{q}_{ext} - p\dot{V} \tag{7}$$

being $\dot{q}_{ext}$ the thermal power exchanged with the metallic surfaces of the cells modeled according to the approach proposed by Tan and Ooi [32].

The convective heat exchange between air and oil is represented by the term $\dot{q}_{air-oil}$. This contribution has a great energy saving potential since it would reduce the compression work $p\dot{V}$: an enhanced air cooling, for instance achieved by spraying the same quantity of oil currently injected to have a greater overall heat exchange surface would lead towards an isothermal compression [33]. Although this technique was also applied in screw [34] and scroll compressors [**? ?**], in sliding vane machines oil injections can be performed along the axial length of the machine such that the residence time of the droplets for the heat exchange is higher, thus the expected cooling effect on the air [35]. The mathematical approach that was used to model the convective heat exchange between air and oil droplets relies on the Spalding low pressure film evaporation theory [36].

$$\dot{q}_{air-oil} = \pi\, D_{drop}\, K_m\, Nu^*\, (T_{air} - T_{drop}) \tag{8}$$

Additional details on the thermal conductivity of the oil-air mixture K_m and the corrected Nusselt number Nu^* that are involved in Equation 8 are provided in [33, 37]. The discriminant parameter for the heat exchange is oil droplet diameter D_{drop}. In the conventional injection technology, as the one on board of the compressor tested for the current study, the lubricant was supplied through calibrated holes which did not succeed to atomize the jet thus to accomplish the desired internal air cooling. This fact, together with the rapidity of the transformation, justified the adiabaticity of the compression noticed experimentally. On the other hand, as it was shown in [35, 37], the usage of pressure swirl nozzles led to finer oil sprays that were able to perform an effective air cooling so reducing the compression work.

Even though volatility and mass diffusivity of the oil used is very low, if the oil partial pressure reached the saturation value at the cell temperature, the lubricant would start to evaporate and gradually lower the cell temperature. This phenomenon is taken into account in the term $\dot{q}_{evap}$, defined as the product of the oil mass flow rate evaporated and the latent heat of vaporization. In this case, the additional need to compress also the oil vapors might reverse the energy benefit. Hence, the oil vaporization should be taken under strict control.

2.4. Lubrication Circuit

In sliding vane compressors, the lubricant is injected inside the cells to mainly fulfill lubrication and sealing purposes. At the discharge, the oil is separated from the mixture with air usually through the mechanical impingement in a labyrinth chamber and a further passage through a coalescence or cyclone separator. The oil is eventually recovered in a tank, as shown by the grey line in Figure 4. The machine layout allows the oil circulation without an auxiliary device: it relies on the pressure difference between the cell pressure at the discharge and the one at the injection angle as driving phenomenon (α_{inj} is reported in Table 1). Hence, the power required to pressurize the oil, that takes into account the compressor efficiency as it was an oil pump, can be calculated according to Eqn. 9.

$$P_{oil} = \frac{Q_{oil}(p_{discharge} - p(\alpha_{inj}))}{\eta_{mech}} \tag{9}$$

In each injector, the oil rate was calculated as through an orifice in steady conditions. This quantity differed from one calibrated hole to the other ones because of the sequence of pressure drops along the oil circuit, whose extensive modeling can be found in [5].

2.5. Friction modeling and blade dynamics

Friction increases the overall energy expenditure for the compressed air production and it is still an open issue for the energy saving in SVRC. Part of the mechanical power supplied is dissipated by friction at the shaft bushes, between the rotor and the side covers of the compressor and because of the blade dynamics. However, the first two phenomena do not produce a noticeable contribution to the overall friction power thanks to the bush technology and to the absence of axial loads from the rotor to the covers [14]. Except for the transient behavior during which oil must be pressurized, friction produced at the bushes is negligible because a dry contact never appears. Hence, the blade dynamics remains the only noteworthy contribution to the power lost by friction.

During its motion, the blade rotates with the rotor and slides along the slot and the inner stator surface: consequently, there are inertial and fictitious forces (centrifugal and Coriolis) acting on it. Since blade thickness and rotor slot width have tight tolerances to prevent leakage flows between consecutive cells, the main degree of freedom of the blade is the translational one along the y direction of Figure 3.a. Hence, the rotational and translational inertias along the x direction were neglected. The power dissipated by friction depends on the reaction forces at the three contact locations, namely 1 and 2 with the side walls of the rotor slot and 3 at blade tip. The blade arrangement inside the rotor slot may assume four configurations: it can be tilted or pushed on the slot walls, either forward or backwards (Figure 3.b). The equilibrium configuration is the one in which all the normal forces are of compression type. From a computational point of view, this depends on the signs of the forces F_1 and F_2 with respect to the configuration shown in Figure 3.a and modeled with the Equations 10 which state the translational equilibria along the x and y directions and the momentum equilibrium respectively.

$$F_1 = F_{pn} - F_{cor} + k_4\, F_c + F_2 + k_2\, F_3 \tag{10a}$$

$$k_1\, F_3 = F_{in} + k_3\, F_c + \lambda\, (F_1 + F_2) \tag{10b}$$

$$\begin{aligned} F_2\, (\lambda\, t_{bl} - (L_{bl} - L_{out})) = F_c(k_4\, (L_{bl}/2 - L_{out}) + ... \\ -k_3\, t_{bl}/2) - F_{pn}\, L_{out}/2 - F_{in}\, t_{bl}/2 + ... \\ -F_{cor}(L_{bl}/2 - L_{out}) - F_3\, (k_2\, L_{out} - k_1\, t_{bl}/2) \end{aligned} \tag{10c}$$

Friction power is also related to the slip velocities of the contact points whose main influencing parameters are rotational speed and compressor aspect ratio, Eqn. 11.

$$P_{fr} = \lambda(F_3\, U + v_{bl}(F_1 + F_2)) \tag{11}$$

Moreover, while the blade tip velocity U is always concordant with the angular velocity ω, the sliding velocity v_{bl} inverts its direction during a complete rotation since the blades come out from the rotor slot during the first half of the cycle and get in during the second half. The tilt angle ϕ eventually affects the load along the directions parallel and orthogonal to the slot axis through the projection angles χ and ξ that in Eqns. 10 are grouped inside the projection coefficients k_{1-4}, whose mathematical formulations are reported in Eqns. 12. Therefore, a modified friction power distribution and a different blade positioning inside the slot may be achieved.

$$k_1 = cos\xi + \lambda\, sign(\phi)\, sin\xi + \lambda\, (1 - |sign(\phi)|)\, sign(sin(\alpha))\, sin(\xi) \tag{12a}$$

$$k_2 = \lambda\, cos\xi - sign(\phi)\, sin\xi - (1 - |sign(\phi)|)\, sign(sin(\alpha))\, sin(\xi) \tag{12b}$$

$$k_3 = cos\chi \tag{12c}$$

$$k_4 = sign(\phi)\, sin\chi \tag{12d}$$

Once blade loads and slip velocities were known, a deeper analysis was performed at the contact between blade tip and the inner stator wall. The lubrication regime was considered hydrodynamic [38]: indeed, the blade tip profile and its motion with respect to the stator pressurize the oil layer as it happens in a plane (or curved) hydrodynamic bearing. Neglecting the effect of eccentricity on the curvature of the stator surface and the transversal variation of oil pressure, at a given angular location of the contact the one-dimensional formulation of the Reynolds equation, that embeds both the continuity and momentum equations, assumed the following expression:

$$\frac{d}{dx}\left(\frac{h^3}{12\mu}\frac{dp}{dx}\right) = \frac{w}{2}\frac{dh}{dx} \tag{13}$$

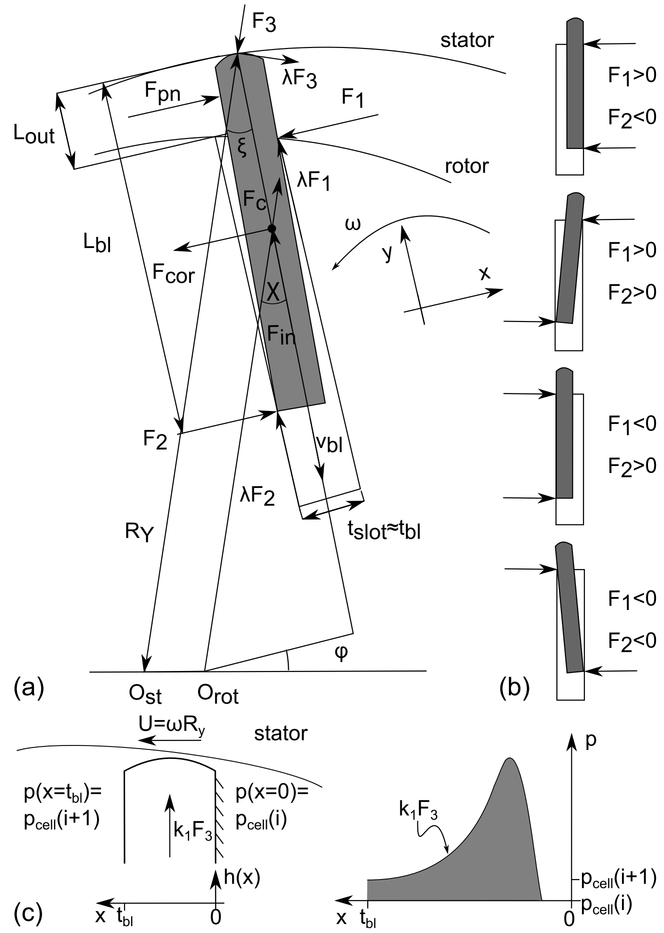

Figure 3: Blade dynamics - Free body diagram (a), possible blade arrangements inside the rotor slot (b) and reference scheme for the analysis of the hydrodynamic lubrication between blade tip and stator wall (c)

being p the pressure realized inside the oil layer and μ the dynamic viscosity of the oil, a key parameter for the lubrication phenomena which is strongly dependent on the oil temperature. However, measurements revealed that the oil temperature from the injection angle until the discharge with the compressed air did not increase significantly (from $72°C$ to $83°C$) because of the thermostatic effect of the metallic surfaces of the machine and the high heat capacity of the lubricant. This allowed to simplify the calculation neglecting the thermal analysis and using a value for the lubricant viscosity calculated at the mean operative temperature.

The oil film thickness $h(x)$ depends on the mutual curvature between stator wall and blade tip profile at a given angle which is known from the compressor geometry considering a unique radius of curvature for the blade tip shape. This parameter, together with blade width, influences the oil film thickness distribution but does not affect the blade load as long as the lubrication regime stays hydrodynamic. On the other hand, sharp and thin blade tip profiles would ease the penetration within the the oil layer and lead to dry contacts.

Within the hydrodynamic assumption, the oil pressure distribution balances the blade load: the integral effect of the oil pressure distribution over the whole contact surface (whose length is the stator one L_{st}) is indeed the orthogonal component of the reaction force at the blade tip $k_1\,F_3$ calculated with Eqn. 10.c.

$$\int_0^{t_{bl}} p(x)\,L_{st}\,dx = k_1\,F_3 \tag{14}$$

The pressures of the consecutive cells separated by the blade act as boundary conditions for the Reynolds equation, as shown in Figure 3.c. Equation 13 was solved considering a quasi-steady approach: for each blade position at a given angle $\tilde{\alpha}$ of the rotation cycle, the pressure boundary conditions imposed by the vanes were considered constant in time as well as the normal blade load and slip velocity at the tip. The resulting pressure distribution is reported in Eqn. 15:

$$p(x,\tilde{\alpha}) = p_{cell,i}(\tilde{\alpha}) + \int_0^{x} \frac{6\,\mu\,U(\tilde{\alpha})}{h^2(x,\tilde{\alpha})}\left(1-\frac{h_0(\tilde{\alpha})}{h(x,\tilde{\alpha})}\right)dx \tag{15}$$

where h_0 is the thickness at which the oil pressure reaches the maximum value. This value results from Equation 16 knowing the pressure boundary conditions and the geometry of the contact:

$$h_0(\tilde{\alpha}) = \frac{\int_0^{t_{bl}} h^{-2}(x,\tilde{\alpha})\,dx - (p_{cell,i+1}(\tilde{\alpha}) - p_{cell,i}(\tilde{\alpha}))/(6\,\mu\,U(\tilde{\alpha}))}{\int_0^{t_{bl}} h^{-3}(x,\tilde{\alpha})\,dx} \tag{16}$$

In this way, the pressure distribution along the contact surface and the minimum oil film thickness were calculated over the whole rotation cycle: this value must be above a minimum threshold to prevent scuffing or excessive wear at the stator during the machine operation.

3. Test setup

An experimental campaign was performed on a mid-size industrial compressor whose geometry is synthesized in Table 1. The machine was instrumented with a set of T-type thermocouples along the air and oil paths as shown in Figure 4.a, while low frequency transducers provided pressure data at the inlet and outlet sections of the compressor.

stator diameter	$136\,mm$	intake port start	30°
rotor diameter	$111\,mm$	intake port end	162°
axial length	$275\,mm$	exhaust port start	325°
blade thickness	$5\,mm$	exhaust port end	356°
blade height	$38\,mm$	injection angle	248°
blade mass	$0.35\,kg$	number of cells	7

Table 1: Geometrical features of the compressor tested

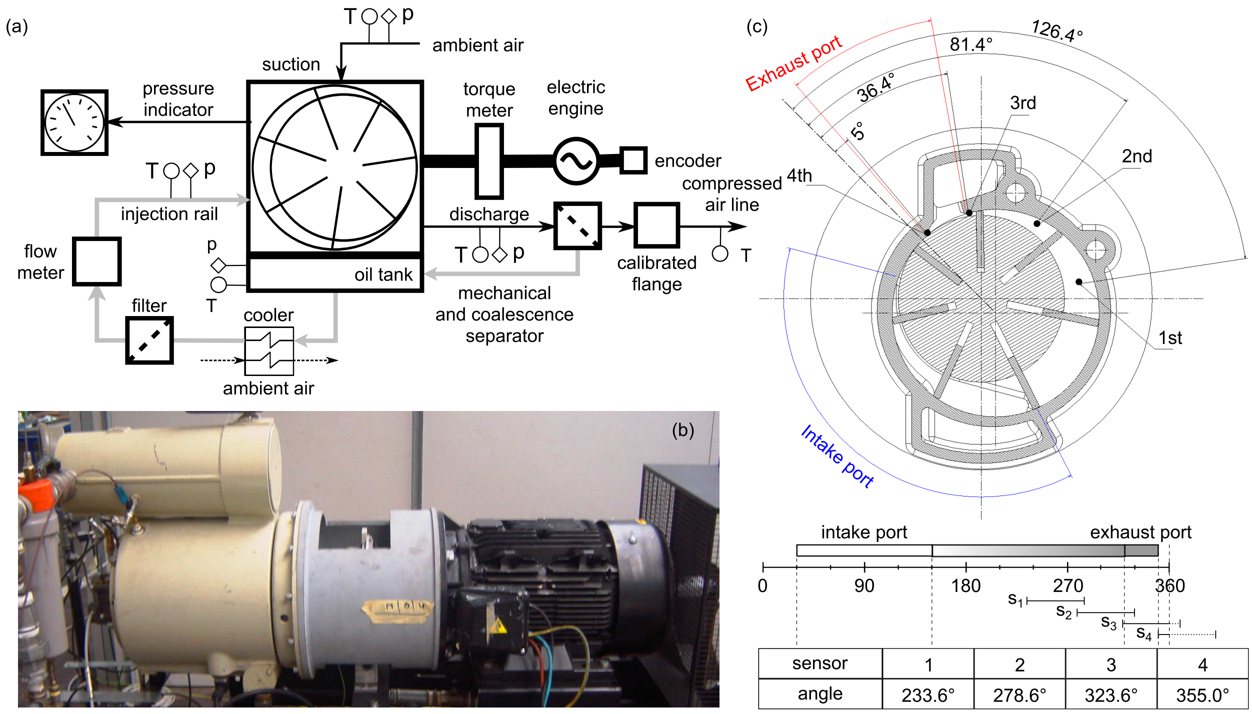

Figure 4: Experimental setup - transducers layout (a), test bench (b), piezoelectric sensors positioning (c)

The relevant feature of the experimental methodology lies on the accurate estimation of the mechanical efficiency of the compressor: the mechanical power (P_{mech}) was evaluated from the product of torque and revolution speed measured through a flange torque meter installed between the compressor and the electric motor (Figure 4.b). On the other hand, compression power was retrieved through the reconstruction of the indicator diagram from the pressure traces given by a set of piezoelectric transducers.

The sensors were installed flush mounted on a side cover of the compressor, circumferentially displaced between stator and rotor. For each of them, the measuring range is equal to the angular extent of the compressor vane ($\Delta\alpha = 360°/N$): with reference to the same rotating cell, the transducer starts to measure when the first blade with respect to the direction of rotation crosses it and ends when the second blade leaves it. The angular position of each transducer, quoted in Figure 4.c, was carefully chosen to enhance the unsteady phenomena that characterize the compressor. These mainly happen during the discharge phase because of the difference between pressure realized by the volumetric ratio of the machine and the one of the compressed air line. Since the discharge port has an angular extent (31°) lower than the measuring range $\Delta\alpha$, two cells discharge at the same time. For these reasons, when the process starts, during an angular displacement equal to 6.5° two sensors (2, 3) measure the same pressure, so detailing the most important unsteady phenomenon. Afterwards, sensors # 3 and # 4 measure the pressure inside the discharging cells and inside the exhaust port. In order to reconstruct the cell pressure evolution over a whole rotation, the relative pressure signals from piezoelectric transducers were referenced to the absolute values measured at the inlet and outlet of the compressor core. Different pressure offsets were applied to each signal such that a matching of the intake and discharge pressures as well as in the overlapping ranges between consecutive transducers was achieved. To further refer the reconstruction procedure to a given angle, a magnetic incremental encoder was used following the experimental methodology proposed in [23]. This device was installed on the shaft of the electric motor that was directly connected to the compressor one. The aim of the angle measurement is twofold: it allows to discriminate which part of the signals happened during the same cycle and it provides the angle evolution versus time, so taking into account the little changes of the angular velocity during a cycle that could lead to different angular displacements in the sampling period (0.1 ms). In order to compensate the effects of cyclic dispersion from one vane to the other, a phase-locked average was performed. The complete pressure trace over the whole rotation was reconstructed assuming the intake process as isobaric while the angular phase between discharge end and intake start, in which the cell crosses the tangency between rotor and stator, was considered as an adiabatic transformation because of the limited extent and the velocity of the transformation. The indicator diagram was eventually reconstructed associating the pressure-angle trace to the volume-angle graph. The reconstruction methodology was applied on the averaged signals and checking the first and second derivatives while performing the overlapping.

In order to evaluate the measurement uncertainty related to the indicated power, the concept of indicated mean effective pressure (IMEP) was used. This quantity is defined as the average pressure which, when multiplied by the vane swept volume, would require the same work out of the cycle as the real pressure of the indicator diagram. The uncertainty on the indicated power was defined as the ratio between the piezoelectric transducers uncertainty (0.125 bar) and the value of IMEP in each test. Hence, a conservative estimation can be safely quantified in the 5 % of the measured value. On the other hand, the direct measurement of the mechanical power allowed to reduce the uncertainty on this quantity to 0.2 % while the value related to the mass flow rate measurement through the calibrated flange (ISA 1392 nozzle) was estimated 4 % according to EN ISO 5167-3.

4. Experimental Results and Model Validation

The compressor performance was investigated at different operating points listed in Table 2. The outlet pressure was varied acting on the set point of the discharge valve while a change in the revolution speed was performed by means of an inverter.

Figure 5 reports the comparison between experimental and simulated indicator diagrams for all the test cases. As it can be noticed from the solid lines, even at 1000 RPM the magnitude of the revolution speed narrows the cycle time for heat transfer to occur and leads to an adiabatic compression phase regardless of the outlet pressure level. On the other hand, the difference between the outlet pressure and the cell pressure

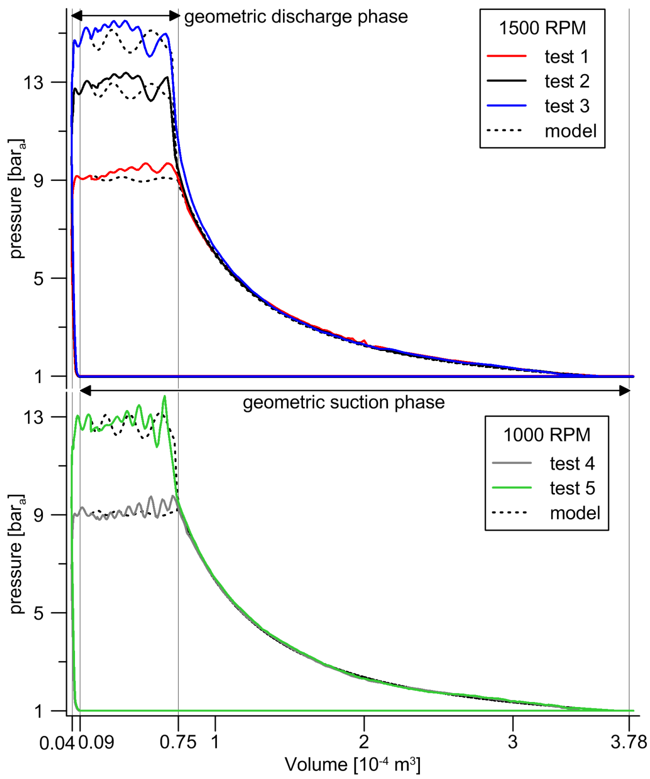

Figure 5: Experimental and simulated indicator diagrams at the operating points listed in Table 2

at the beginning of the discharge process affects the last part of the compression phase and triggers pressure oscillations during the exhaust whose magnitude is proportional to the pressure gap itself. Indeed, this phenomenon is highly remarkable at 12.5 bar and 14.5 bar. The pressure step involved at the end of the compression phase deviates from the theoretical isochoric trend because of the dynamics of the discharge valve. The model calculations, displayed with a dashed line in Figure 5, show a satisfactory agreement with the experimental data although the pressure unsteadiness is not fully predicted.

The analysis of experimental data also allowed to calculate the volumetric efficiency of the machine as the ratio of the actual mass flow rate measured and the theoretical value that depends on the volumetric capacity of the machine and the air density at the suction process, as expressed by Eqn. 17.

$$\eta_{vol} = \frac{60\,\dot{m}_{measured}}{\rho_{suc}\,N\,\omega\,V_{suc}} \tag{17}$$

where the units of the revolution speed ω are RPM and V_{suc} is the cell volume at the end of the suction process ($\alpha_{suc} = 162° + \Delta\alpha$ since it refers to the second blade of the cell with respect to the rotation sense). The values reported in Table 2 show a strong influence of the suction temperature on the volumetric efficiency of the compressor because it directly affects the inlet density ρ_{suc}: in test # 2, η_{vol} drops of almost 6 % compared to test # 1 that is at the same revolution speed. For similar suction temperatures ($43.4°C$

		test 1	test 2	test 3	test 4	test 5
discharge pressure	bar$_a$	8.93	12.50	14.52	8.94	12.51
revolution speed	RPM	1470	1451	1455	995	981
mass flow rate	kg/s	0.067	0.057	0.063	0.046	0.044
indicated power	kW	18.86	21.82	23.71	12.90	14.79
mechanical power	kW	21.85	25.37	27.61	14.58	17.05
suction temperature	$°C$	43.4	62.8	49.5	51.8	57.0
volumetric efficiency	%	94.0	88.1	91.9	96.7	96.4

Table 2: Experimental compressor performance at various discharge pressures and revolution speeds

- 49.5$°C$ at 1500 RPM and 51.8$°C$ - 57$°C$ at 1000 RPM), the volumetric efficiency slightly decreases at higher outlet pressures. This effect was expected due to the leakage flows between contiguous cells. However, in sliding vane compressors the effect of oil sealing is remarkable and led to these minor variations. This fact is in agreement with the assumption made when neglecting leakages in the compressor model. The experiments eventually state an increase of the volumetric efficiency at lower revolution speeds.

Figure 6 summarizes the model validation comparing experimental and simulated values concerned to synthetic parameters that quantify the compressor performance, namely mass flow rate and indicated power. The latter quantity is calculated from the area of the indicator diagram and the blade passing frequency using Eqn. 18:

$$P_{ind} = N \frac{\omega}{60} \oint p \, dV \tag{18}$$

Both simulated quantities falls within the uncertainty band of the measured data in all the test cases and state the confidence and reliability of the model.

From the energy balance at the compressor, whose expression is reported in Eqn. 19, only part of the mechanical power supplied is converted into indicated power and it is so used to compress the air; the remaining contribution accounts for the dissipations by friction (Eqn. 11) and the power needed to pressurize the oil (Eqn. 9).

$$P_{mech} = P_{ind} + P_{fr} + P_{oil} \tag{19}$$

Since P_{mech} and P_{oil} were available from the experiments, once the indicator diagrams were reconstructed, the friction coefficient λ in Eqn. 11 could be estimated in 0.065 for all the test cases.

The model calibration and validation allowed to reproduce the compressor performance map: Figure 7 shows the air mass flow rate delivered at different outlet pressure levels and revolution speeds. As occurred in the experiments reported in Table 2, the suction conditions highly affect the volumetric efficiency of the

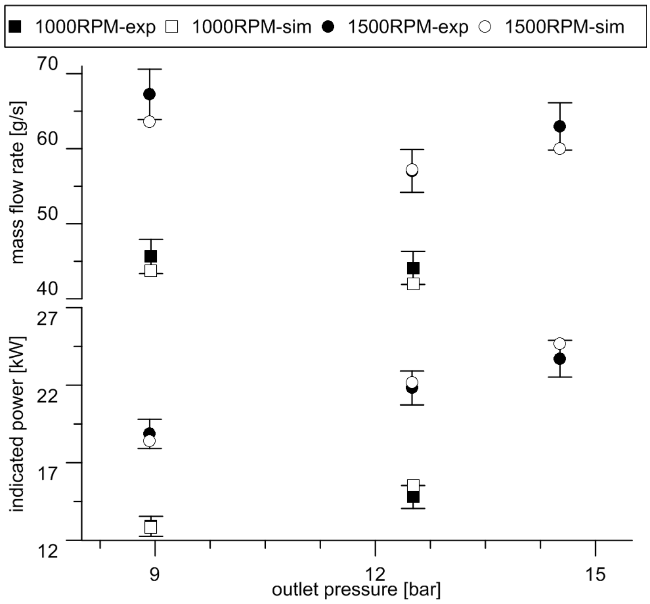

Figure 6: Model validation

compressor since they directly act on the inlet air density; for these reasons, the chart refers to ISO 1217 conditions (1 bar, $20°C$). The volumetric nature of the machine is stated by the linear dependance of the mass flow rate with the revolution speed. Additionally, the effect of the delivery pressure on the volumetric efficiency of the machine can be noticed with reference to the slope of the performance curves at constant speed: the higher is the compression ratio, the lower is the mass flow that the compressor can elaborate.

5. Parametric analysis for the performance optimization

In order to address future performance enhancements for the sliding vane compressor technology, a parametric study was carried out using the simulation platform developed. The reference adopted is the test case #1 in Table 2, a typical operating condition of the compressor in industrial applications. The analysis aimed at maximizing the mechanical efficiency of the compressor, defined as the ratio of the power that is actually used for the air compression and the overall mechanical power supplied (Eqn. 20).

$$\eta_{mech} = \frac{P_{ind}}{P_{mech}} \tag{20}$$

Figure 8 shows the effects of varying either the stator or the rotor diameter on the compressor aspect ratio and friction power. To keep the reference mass flow rate, axial length of the compressor was varied accordingly. The resulting machine layouts are of two categories: an elongated one, in which the axial length is predominant with respect to the radial extent and a flat one which exhibits bigger diameters and shorter lengths than the actual geometry reported in Table 1. A reduction of the stator diameter limits the

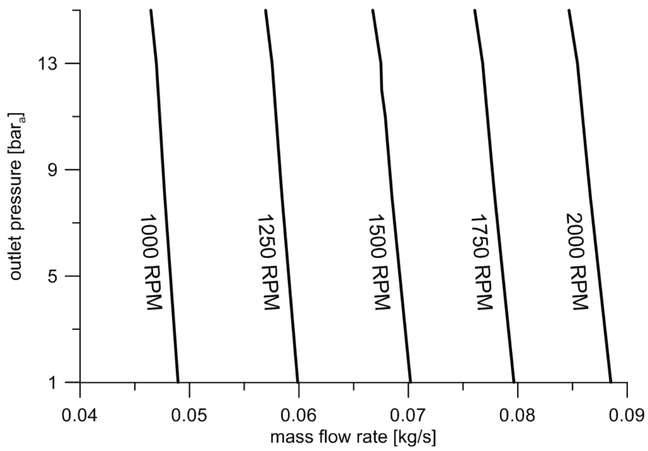

Figure 7: Simulated compressor performance map at ISO 1217 suction conditions (1 bar, 20°C)

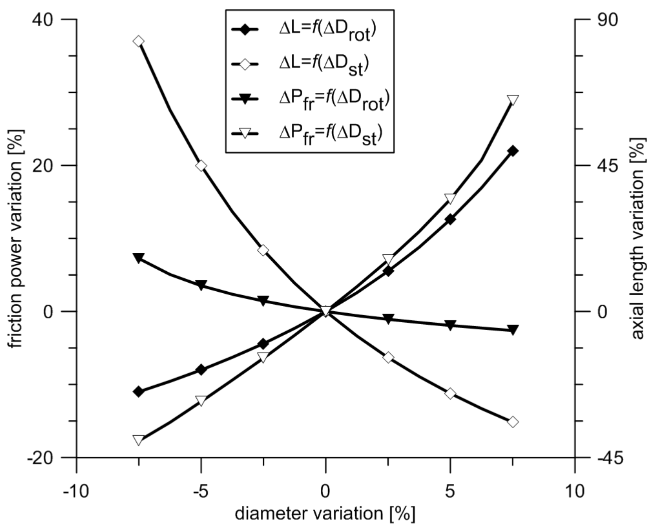

Figure 8: Influence of the aspect ratio on the compressor geometry and friction power dissipated

peripheral tip speed (U) and leads to a reduction of the most significant contribution to the friction power. On the other hand, being the revolution speed kept constant, a decrease in the rotor diameter results in an increase of the sliding velocity v_{bl}, since the displacement that the blades have to accomplish in the same amount of time (i.e. the revolution period) increased. Even if this contribution has a minor importance compared to the one at the tip, a worsening of the mechanical efficiency would result from this aspect ratio.

A combined analysis on the effects of revolution speed and blade tilt on the mechanical efficiency of the compressor is reported in Figure 9 in terms of specific power dissipated by friction with forward and backward blade tilt varying the angular velocity from 1000 RPM to 2000 RPM. The reduction of revolution speed has a direct and significant effect on friction power since it reduces both the inertial and fictitious forces as well as all the slip velocities. This methodology cannot be applied to other rotary volumetric

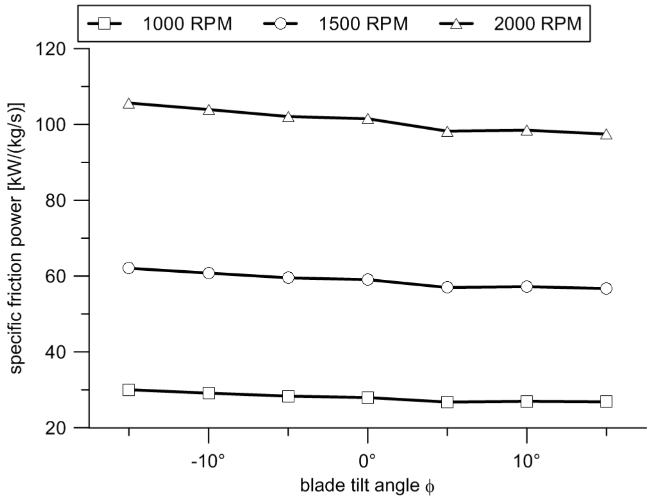

Figure 9: Variation of the friction power per unit air delivered with revolution speed and blade tilt

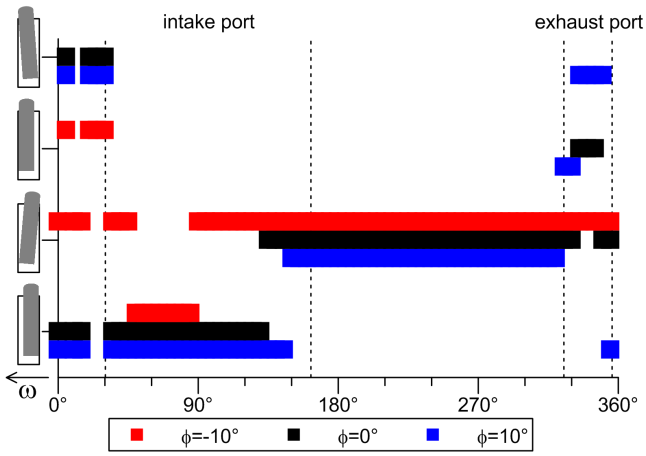

Figure 10: Blade positioning inside the rotor slot for radial and non-radial configurations

compression technologies (e.g. screw) and becomes a distinguishing feature of sliding vane machines. The results presented are in agreement with the experimental data of Tramschek and Mkumbwa who tested a circular sliding vane compressor with radial and non-radial blades [22]. The energy benefit that might be achieved with forward-backward blade tilting is hardly noticeable, especially at low speeds.

However, the non-radial blade arrangement affects the load distribution on the blade since both the active and reaction forces involved are differently projected along the symmetry axes of the blade, as in Figure 3. This fact leads to another force balance, thus to a modified positioning inside the rotor slot, as displayed in Figure 10. With reference to the radial configuration (ϕ=0), at the intake the side walls of the blade are both exposed to the suction pressure. Therefore, inertial and fictitious forces become predominant and push the blade backward onto the rotor slot. As the compression starts, the pressure difference between the

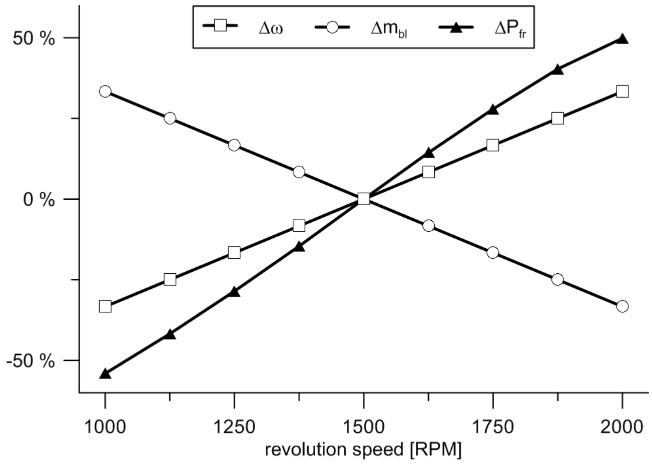

Figure 11: Effects of the revolution speed on the overall blade mass and friction power with respect to test case # 1 in Table 2

side walls tilts the blade towards the rotation sense and makes it to assume the configuration reported in Figure 3. The angular extent in which the blade assumes this position is amplified for forward blade tilt ($\phi > 0$) and reduced for backward tilt ($\phi < 0$). The pressure unsteadiness that characterize the discharge and the passage across the tangency between stator and rotor leads the blade to assume all the possible configurations. The combined examination of Figures 9 and 10 allowed to state that blade tilt does not effectively contribute to achieve an improvement of the mechanical efficiency of the compressor since it does modify the blade load distribution but without affecting the slip velocities at the friction locations.

Being the highest slip velocity at the contact point between blade tip and stator wall, the main contribution to the overall friction power dissipated was deeply investigated varying the mass of the compressor blade and revolution speed. Since the latter parameter directly affects the flow rate delivered by the machine, the axial length of the compressor was varied to keep the reference test conditions. Using the same linear density for the blade, the length adjustment led to heavier (longer) blades whether the revolution speed was lower than 1500 RPM and to lighter machines at revolution speeds higher than the reference value.
Although both mass and revolution speed affect the friction power, while the mass dependence is linear, the effects of revolution speed are more noticeable since they have a quadratic trend on the centrifugal force as well as a linear influence on the slip velocities at all the contact points. However, as displayed in Figure 11, if the volumetric capacity of the machine is kept constant, the blade mass varies with an opposite trend with respect to the revolution speed. Hence, the benefits of lowering the angular velocity of the machine onto the friction power become linear.

Using the simulation approach of Figure 11, a further analysis was performed at the same revolution speeds additionally aiming at addressing the benefits of a blade mass reduction. This could be achieved through a mechanical removal of some material from the current blades or using unconventional materials able to match the lubrication issues. The results displayed in Figure 12 are reported in terms of minimum

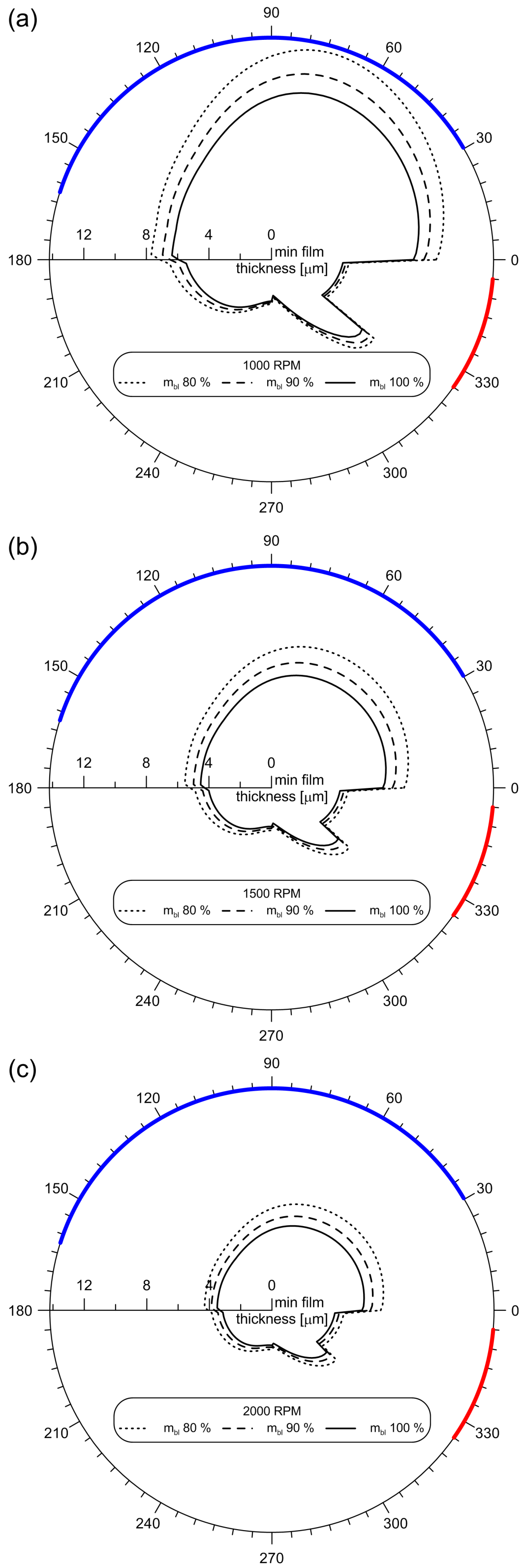

Figure 12: Effects of the blade mass reduction on the minimum thickness of the oil film established between the blade tip and the stator wall at 1000 (a), 1500 (b) and 2000 RPM (c)

value of the oil film thickness to highlight the hydrodynamic capabilities of the lubricant layer in withstanding the blade load. Furthermore, this parameter is inversely proportional to the maximum pressure along the contact surface. All the simulations show that the oil film thins during the second half of the rotation since the inertia force becomes concordant to the centrifugal force (as in Figure 3) increasing the blade load at the tip. The highest stress is reached when the vane pressure is maximum, i.e. before the cell opens towards the exhaust port. The location of the minimum film thickness is anticipated of $\Delta\alpha$ in Figure 12 since the graph refers to the second blade of the cell with respect to the rotation sense. The exhaust opening produces a discontinuity, thanks to which minimum thickness increases. During this phase, indeed, pressure forces acting on the lateral blade surfaces are equal and this reduces $k_1\, F_3$ term. The blade result less loaded and oil thickness tends to increase. When the exhaust port is closed the remaining air is pressurized and the minimum thickness reassumes the values it had before the port opening. On the other hand, during the suction process, both sides of the blade are again exposed to the same pressure performing a reduction of the load at the blade tip that ends up in a thickening of the oil film.

When the revolution speed increases, the minimum thickness decreases being the effects of the centrifugal force more severe. Hence, critical operating conditions get closer, opening the way to possible dry contacts. Furthermore, at any revolution speed, lighter blades lead to thicker oil layers thus to a decrease in the orthogonal load between the blade tip and the stator wall. In this way, a reduction of the friction power dissipated might be achieved. However, these actions need to deal with the blade stability and sealing issues to prevent mass leakages between adjacent vanes.

6. Conclusions

Sliding vane rotary compressors might represent an astonishing technology to accomplish energy saving commitments in compressed air systems. The current work investigated the peculiar features of these machines from theoretical and experimental viewpoints aiming at characterizing the compressor energy performance and addressing improvements of the mechanical efficiency.

The comprehensive mathematical model developed considers all the relevant phenomena involved in a sliding vane rotary compressor. The geometry was modeled to explore any machine configuration: backward and forward blade tilt can be simulated as well as suction and exhaust ports with an axial or radial arrangements. The flow dynamics was investigated using a quasi-propagatory approach that takes into account the inertial, capacitive and resistive features of the flow during vane filling and emptying processes. On the other hand, solving the unsteady energy equation at the compressor cells provided the pressure evolution over the whole rotation cycle. The blade dynamics and the analysis of the hydrodynamic lubrication between blade tip and stator wall were eventually implemented to characterize the friction power dissipated, thus the mechanical efficiency of the compressor.

strategy	design parameter change	η_{mech}
test #1 Table 2	reference	86.3%
aspect ratio	-5% D_{st}, + 45% L_{st}	88.0%
blade tilt	+10°	86.8%
revolution speed + blade tilt	1000 RPM, +10°	95.5%
revolution speed, constant blade mass	1000 RPM	95.2%
revolution speed, variable blade mass	1000 RPM, +50% m_{bl}	91.5%

Table 3: Optimization summary

An experimental test campaign on a mid-size industrial compressor at different revolution speeds (1000 and 1500 RPM) and discharge pressures (9, 12.5 and 14.5 bar) was further carried out using a set of piezoelectric transducers to retrieve the indicator diagram. The narrow time cycle led to an adiabatic compression phase in all the test cases while the outlet pressure value influenced the unsteadiness during the discharge process. Hence, the indicated power and the mass flow rate measured validated the model results with simulated values within the uncertainty bands and provided an estimation of the friction coefficient of 0.065.

The simulation platform was ultimately used to investigate geometrical and operating parameters of the compressor to maximize its mechanical efficiency (Table 3). Since friction power dissipated between blade tip and stator wall is the most significant contribution, a change in the compressor aspect ratio would result effective whether a reduction of the stator diameter was realized. Accordingly, a reduction of the blade mass would decrease the reaction force at the blade tip that balances the centrifugal effects while decreasing the revolution speed would also act on the slip velocities. However, these actions need to be applied without affecting the vane sealing and blade stability. Although the blade positioning inside the rotor slot during a whole rotation is affected by a forward or backward blade tilt, a noticeable effect on the overall friction power dissipated is not achieved: the blade tilt affects the load distribution but does not modify the slip velocity at the friction contact points. The oil layer at blade tip, that assures the sealing between vanes, assumes its most critical conditions when the blade is approaching the exhaust port. Operating conditions at lower revolution speed and lighter blades would favor the hydrodynamic lubrication and keep the minimum oil film thickness above a safety threshold to prevent dry contacts with the stator wall.

Acknowledgement

The Authors acknowledge Ing. E. Mattei S.p.A. and particularly its CEO, Dr. Giulio Contaldi, for continuous research funding and support. The work has been done also under the FP7 Project "Complete Vehicle Energy-Saving CONVENIENT" founded by the European Commission.

References

[1] P. Radgen, Compressed air systems in the European Union: energy, emissions, savings potential and policy actions, LOG_X Verlag GmbH, 2001.

[2] R. Saidur, N. Rahim, M. Hasanuzzaman, A review on compressed-air energy use and energy savings, Renewable and Sustainable Energy Reviews 14 (4) (2010) 1135 – 1153. doi:10.1016/j.rser.2009.11.013.

[3] R. Cipollone, Sliding vane rotary compressor technology and energy saving, Proceedings of the Institution of Mechanical Engineers, Part E: Journal of Process Mechanical Engineeringdoi:10.1177/0954408914546146.

[4] O. Badr, P. O'Callaghan, S. Probert, Multi-vane expanders: Geometry and vane kinematics, Applied Energy 19 (3) (1985) 159 – 182. doi:10.1016/0306-2619(85)90006-6.

[5] R. Cipollone, G. Contaldi, A. Sciarretta, R. Tufano, C. Villante, A theoretical model and experimental validation of a sliding vane rotary compressor, in: Proceedings of the International Compressor Engineering Conference, Purdue University, 2006.
URL http://docs.lib.purdue.edu/icec/1755/

[6] W. Reed, J. Hamilton, Internal leakage effects in sliding vane, rotary compressors, in: Proceedings of the International Compressor Engineering Conference, Purdue University, 1980.
URL http://docs.lib.purdue.edu/icec/316/

[7] R. Valente, C. Villante, On the optimal design of one-rotor two-stages rotary-vane compressors, in: Proceedings of the International Compressor Engineering Conference, Purdue University, 2008.
URL http://docs.lib.purdue.edu/icec/1895/

[8] X. Tojo, T. Kan, A. Arai, Dynamic behavior of sliding vane in small rotary compressors, in: Proceedings of the International Compressor Engineering Conference, Purdue University, 1978.
URL http://docs.lib.purdue.edu/icec/242/

[9] A. Tramschek, M. Mkumbwa, Mathematical modelling of radial and non-radial rotary sliding vane compressors, in: Proceedings of the International Compressor Engineering Conference, Purdue University, 1996.
URL http://docs.lib.purdue.edu/icec/1151/

[10] T. Brown, V. Atluri, J. Schmiedeler, A low-cost hybrid drivetrain concept based on compressed air energy storage, Applied Energy 134 (0) (2014) 477 – 489. doi:10.1016/j.apenergy.2014.07.111.

[11] J. Lozano, K. Engelbrecht, C. Bahl, K. Nielsen, D. Eriksen, U. Olsen, J. B. Jr., A. Smith, A. Prata, N. Pryds, Performance analysis of a rotary active magnetic refrigerator, Applied Energy 111 (0) (2013) 669 – 680. doi:10.1016/j.apenergy.2013.05.039.

[12] D. Aradau, L. Costiuc, Friction power in sliding vane type rotary compressors, in: Proceedings of the International Compressor Engineering Conference, Purdue University, 1996.
URL http://docs.lib.purdue.edu/icec/242/

[13] L. Li, Y. Zhao, B. Guo, P. Shu, J. Shen, S. He, Wrap of cylinder and its effect on main features of rotary vane compressor for automobile air conditioning system, International Journal of Refrigeration 26 (5) (2003) 566 – 574. doi:10.1016/S0140-7007(02)00148-2.

[14] O. Badr, S. Probert, P. O'Callaghan, Multi-vane expanders: Vane dynamics and friction losses, Applied Energy 20 (4) (1985) 253 – 285. doi:10.1016/0306-2619(85)90018-2.

[15] Y. Teh, K. Ooi, Theoretical study of a novel refrigeration compressor part i: Design of the revolving vane (rv) compressor and its frictional losses, International Journal of Refrigeration 32 (5) (2009) 1092 – 1102. doi:10.1016/j.ijrefrig.2008.09.006.

[16] H. Lindemann, H. Kaiser, M. Kuever, H. Kruse, Optimization of a special shaped rotary vane compressor-comparison of theoretical and experimental results, in: Proceedings of the International Compressor Engineering Conference, Purdue

University, 1982.
URL http://docs.lib.purdue.edu/icec/393/

[17] H. Platts, Hydrodynamic lubrication of sliding vanes, in: Proceedings of the International Compressor Engineering Conference, Purdue University, 1976.
URL http://docs.lib.purdue.edu/icec/187/

[18] O. Al-Hawaj, Theoretical modeling of sliding vane compressor with leakage, International Journal of Refrigeration 32 (7) (2009) 1555 – 1562. doi:10.1016/j.ijrefrig.2009.07.005.

[19] H. Kruse, Experimental investigations on rotary vane compressors, in: Proceedings of the International Compressor Engineering Conference, Purdue University, 1980.
URL http://docs.lib.purdue.edu/icec/318/

[20] Y. S. Park, J. H. Jeong, B. H. Ahn, Heat pump control method based on direct measurement of evaporation pressure to improve energy efficiency and indoor air temperature stability at a low cooling load condition, Applied Energy 132 (0) (2014) 99 – 107. doi:10.1016/j.apenergy.2014.07.011.

[21] M. Antonelli, L. Martorano, A study on the rotary steam engine for distributed generation in small size power plants, Applied Energy 97 (0) (2012) 642 – 647, energy Solutions for a Sustainable World - Proceedings of the Third International Conference on Applied Energy, May 16-18, 2011 - Perugia, Italy. doi:10.1016/j.apenergy.2011.11.054.

[22] A. Tramschek, M. Mkumbwa, Experimental studies of non-radial vane rotary sliding vane air compressors during steady state operation, in: Proceedings of the International Compressor Engineering Conference, Purdue University, 1996.
URL http://docs.lib.purdue.edu/icec/1152/

[23] Y. M. Huang, S.-A. Yang, A measurement method for air pressures in compressor vane segments, Measurement 41 (8) (2008) 835 – 841. doi:10.1016/j.measurement.2005.11.027.

[24] B. Yang, X. Peng, Z. He, B. Guo, Z. Xing, Experimental investigation on the internal working process of a co_2 rotary vane expander, Applied Thermal Engineering 29 (1112) (2009) 2289 – 2296. doi:10.1016/j.applthermaleng.2008.11.023.

[25] M. Antonelli, A. Baccioli, M. Francesconi, U. Desideri, L. Martorano, Operating maps of a rotary engine used as an expander for micro-generation with various working fluids, Applied Energy 113 (0) (2014) 742 – 750. doi:10.1016/j.apenergy.2013.08.003.

[26] V. Yee, W. Soedel, Pressure oscillations during re-expansion of gases in rotary vane compressors by a modified helmholtz resonator approach, Journal of Sound and Vibration 91 (1) (1983) 27 – 36. doi:10.1016/0022-460X(83)90448-0.

[27] Y.-C. MA, O.-K. MIN, Pressure calculation in a compressor cylinder by a modified new helmhotz modelling, Journal of Sound and Vibration 243 (5) (2001) 775 – 796. doi:10.1006/jsvi.2000.3477.

[28] R. Cipollone, D. Vittorini, Energy saving potential in existing compressors, in: Proceedings of the 22nd International Compressor Engineering Conference, Purdue University, 2014.

[29] D. Vittorini, G. Bianchi, R. Cipollone, Energy saving potential in existing volumetric rotary compressors, in: Proceedings of the 69th Conference of the Italian Thermal Machines Engineering Association, Energy Procedia, 2014.

[30] R. Cipollone, A. Sciarretta, The quasi-propagatory model: A new approach for describing transient phenomena in engine manifolds, SAE Technical Papersdoi:10.4271/2001-01-0579.

[31] R. Cipollone, A. Sciarretta, New modelling for the air and gas dynamics in ice manifolds oriented to air-fuel ratio control, American Society of Mechanical Engineers, Internal Combustion Engine Division (Publication) ICE 32.

[32] K. Tan, K. Ooi, Heat transfer in compression chamber of a revolving vane (rv) compressor, Applied Thermal Engineering 31 (89) (2011) 1519 – 1526. doi:10.1016/j.applthermaleng.2011.01.041.

[33] R. Cipollone, G. Bianchi, G. Contaldi, Sliding vane rotary compressor energy optimization, in: ASME 2012 International Mechanical Engineering Congress and Exposition, American Society of Mechanical Engineers, 2012, pp. 69–80. doi:10.1115/IMECE2012-85955.

[34] M. D. Paepe, W. Bogaert, D. Mertens, Cooling of oil injected screw compressors by oil atomisation, Applied Thermal Engineering 25 (1718) (2005) 2764 – 2779. doi:10.1016/j.applthermaleng.2005.02.003.

[35] R. Cipollone, G. Valenti, G. Bianchi, S. Murgia, G. Contaldi, T. Calvi, Energy saving in sliding vane rotary compressors using pressure swirl oil atomizers, Proceedings of the Institution of Mechanical Engineers, Part E: Journal of Process Mechanical Engineeringdoi:10.1177/0954408914550356.

[36] D. B. Spalding, Theory of particle combustion at high pressures, ARS Journal 29 (1959) 828 – 835. doi:10.2514/8.4918.

[37] G. Bianchi, R. Cipollone, S. Murgia, G. Contaldi, Performance enhancement in sliding vane rotary compressors through a sprayed oil injection technology, in: Proceedings of the 22nd International Compressor Engineering Conference, Purdue University, 2014.

[38] M. Fowell, S. Medina, A. Olver, H. Spikes, I. Pegg, Parametric study of texturing in convergent bearings, Tribology International 52 (0) (2012) 7 – 16. doi:10.1016/j.triboint.2012.02.013.

List of symbols

α	angular coordinate	$[rad]$
γ	specific heat ratio	$[-]$
ξ	contraction ratio	$[-]$
η	efficiency	$[-]$
λ	friction coefficient	$[-]$
μ	oil dynamic viscosity	$[Pa\,s]$
ζ	force projection angle	$[rad]$
ρ	density	$[kg/m^3]$
τ	QPM parameter	$[s]$
ϕ	blade tilt angle	$[rad]$
χ	force projection angle	$[rad]$
ω	revolution speed	$[RPM]$
Λ	QPM parameter	$[-]$
Ω	QPM parameter	$[s^{-1}]$
a	speed of sound	$[m/s]$
h	film thickness	$[m]$
k	force projection coefficient	$[-]$
m	mass	$[kg]$
p	pressure	[Pa]
q	heat flux	[J]
t	thickness	$[m]$
u	flow velocity	$[m/s]$
v	slip velocity	$[m/s]$
w	oil flow velocity	$[m/s]$
A	upstream boundary condition slope	$[N\,s/m^3]$
B	downstream boundary condition slope	$[N\,s/m^3]$
C	characteristic curve slope	$[N\,s/m^3]$
D	diameter	$[m]$
E	absolute internal energy	$[J]$
F	force	$[N]$
H	specific enthalpy	$[J/kg]$
K_m	mixture thermal conductivity	$[W/m/K]$
L	length	$[m]$
N	number of cells	$[-]$
Nu^*	corrected Nusselt number	$[-]$
P	power	$[W]$
Q	flow rate	$[m^3/s]$
R	gas constant	$[J/kg/K]$
R_Y	tip radius	$[m]$
S	duct cross section area	$[m^2]$
T	temperature	$[K]$
U	blade tip speed	$[m/s]$
V	cell volume	$[m^3]$

Subscrips and superscripts

$'$	initial state
0	thickness at maximum pressure
∞	steady state
bl	blade
c	centrifugal
cor	Coriolis
d	downstream
drop	oil droplet
evap	evaporation
ext	external
fr	friction
in	inertia
ind	indicated
inj	injection
inl	inlet
mech	mechanical
out	outside the rotor slot
outl	outlet
pn	normal pressure
st	stator
suc	suction conditions
u	upstream
vol	volumetric

Mathematical operators

$\dot{\Upsilon}$	first time derivative of Υ
$\ddot{\Upsilon}$	second time derivative of Υ